Crystal structure and magnetic properties of Pr- and Ti-substituted La2RuO5

S. Riegg, Alois Loidl, Armin Reller, Stefan G. Ebbinghaus

Angaben zur Veröffentlichung / Publication details:

Riegg, S., Alois Loidl, Armin Reller, and Stefan G. Ebbinghaus. 2013. "Crystal structure and magnetic properties of Pr- and Ti-substituted La2RuO5." *Materials Research Bulletin* 48 (11): 4583–89. https://doi.org/10.1016/j.materresbull.2013.07.054.

Crystal structure and magnetic properties of Pr- and Ti-substituted La_2RuO_5

S. Riegg [a,*], A. Loidl [a], A. Reller [b], S.G. Ebbinghaus [c]

[a] Experimental Physics V, Center for Electronic Correlations and Magnetism, University of Augsburg, D-86159 Augsburg, Germany
[b] Resource Strategy, University of Augsburg, D-86159 Augsburg, Germany
[c] Solid State Chemistry, Martin-Luther University Halle-Wittenberg, D-06099 Halle, Germany

1. Introduction

The layered perovskite-related ruthenate La_2RuO_5 exhibits a (quasi) non-magnetic ground state due to a spin-dimerization transition [1]. To study the nature of the dimerization, a number of investigations have been performed substituting either on the La-site or on the Ru-site [2–4]. La can partly be replaced by various rare-earth elements resulting in $La_{2-x}Ln_xRuO_5$ (*Ln* = Pr, Nd, Sm, Gd, and Dy). Depending on the different lanthanides a maximum substitution limit x was found, which is determined by the difference of the ionic radii of the lanthanides compared to La. For Pr a value of $x_{max} = 0.75$ was obtained, while for Dy the maximum substitution level is already reached for $x_{max} = 0.2$. Furthermore, the substitution of Ru by Ti was successfully carried out leading to samples with the composition $La_2Ru_{1-y}Ti_yO_5$ up to a substitution level of $y = 0.45$ [4]. Both types of substitutions resulted in distinct changes in the dimerization transition, in the magnetic susceptibility, the crystal structure, and the specific heat as described in detail in Refs. [2–6].

* Corresponding author. Tel.: +49 8215983751; fax: +49 8215983649.
E-mail address: stefan.riegg@physik.uni-augsburg.de (S. Riegg).

Pure La_2RuO_5 reveals a magneto-structural phase transition at $T_d = 161$ K. The high-temperature (ht-) paramagnetic phase crystallizes in the monoclinic space group $P2_1/c$ (No. 14). It is a semiconductor with a small band gap of approximately 0.15 eV, as determined from resistivity measurements. In contrast, the low-temperature (lt-) phase provides triclinic symmetry (space group $P\bar{1}$, No. 2), a drastically diminished magnetic susceptibility of approximately 10^{-4} emu/mol and a slightly increased band gap of 0.21 eV [1,7,8]. The almost completely suppressed paramagnetic moment of the lt-phase was reported to result from the formation of non-magnetic Ru–Ru singlets of the Ru^{4+} spin moments ($S = 1$) in a spin-Peierls like transition. The Ru moments arrange antiparallel in dimers forming rungs of two-leg ladders along *c*. This dimerization is triggered by changes in the Ru–Ru distances and Ru–O–Ru bond angles due to a structural phase transition. The spin-Peierls like scenario is supported by various density functional theory calculations [6,9–11].

The crystal structure of Pr- and Ti-substituted La_2RuO_5 is schematically depicted in Fig. 1 using a perspective view along the *c*-axis. La_2RuO_5 can be described by alternating perovskite-like $LaRuO_4$ layers and buckled LaO layers, which are stacked perpendicular to the crystallographic *a*-axis [13]. Concerning the rare-earth substitution a partial cationic ordering in $La_{2-x}Ln_xRuO_5$

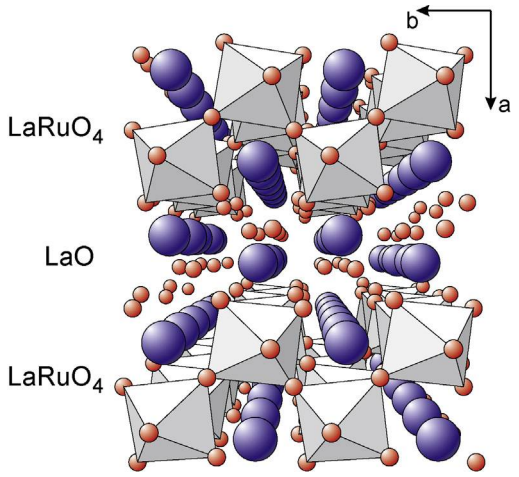

Fig. 1. Crystal structure of $La_{2-x}Pr_xRu_{1-y}Ti_yO_5$ in a pespective view along the *c*-axis. Oxygen is represented by small red spheres and La by large blue spheres. The RuO_6-octahedra in the $LaRuO_4$-layers are colored gray. (For interpretation of the references to color in figure legend, the reader is referred to the web version of the article.)

is found. Approximately two thirds of the incorporated *Ln* are located in the LaO layers, as derived from neutron diffraction and X-ray absorption fine structure (EXAFS) measurements [3,5]. The Ti substitution, on the other hand, does not lead to an ordering effect or the appearance of superstructures in the $La_2Ru_{1-y}Ti_yO_5$ compounds [4].

The rare-earth substitution was found to have only a small impact on the spin-Peierls transition, i.e. Ln^{3+} ions are remaining as isolated paramagnetic centers in the structure and the interaction with the magnetic Ru sublattice is weak [3,6]. In contrast, the Ti substitution effectively disturbs the magnetic Ru–Ru dimerization due to the $3d^0$ configuration of the Ti^{4+} ions. With increasing substitution level the transition temperature decreases and the drop in the magnetic susceptibility becomes smaller until the spin-dimerization completely vanishes for $y = 0.45$, in accordance with the simultaneous suppression of the structural transition. For $y \geq 0.3$ the long-range ordered singlet state transforms into clusters of short-range ordered dimers, resulting in significant changes of the Curie–Weiss temperature at this substitution level and the disappearance of the specific heat anomaly [4].

In the course of these investigations the question arose whether the simultaneous substitution on both the La and Ru positions might result in unexpected new effects. For example, due to magnetic fluctuations caused by the Ti substitution and the remaining unpaired Ru spin moments, new interactions with the magnetic moments of the Pr ions may become possible. Therefore, we prepared a series of Pr and Ti co-doped samples. Their magnetic ground states were characterized by measurements of the magnetic susceptibilities. In addition, the room temperature crystal structures of $La_{2-x}Pr_xRu_{1-y}Ti_yO_5$ were investigated by X-ray powder diffraction, in order to reveal possible correlations between the two different types of substitution.

2. Experimental

For the synthesis of the polycrystalline $La_{2-x}Pr_xRu_{1-y}Ti_yO_5$ compounds a soft chemistry approach is required, since it was found impossible to obtain single phase material from solid-state reactions. The powder samples were synthesized using a sol–gel route based on the thermal decomposition of citrate stabilized precursors. These precursors were prepared according to a recently reported method [4]. $Pr(NO_3)_3 \times 6\ H_2O$ (Chempur, 99.9%) was added in appropriate amounts to the aqueous precursor solutions of citratoperoxotitanate, rutheniumnitrosyleacetate, lanthanum-nitrate-hydrate, and citric acid. From the obtained solutions the solvent was boiled off until gels formed. These gels were decomposed at 600°C and finally calcined at 1175°C for at least 96 hours. The samples were reground every 48 h. The calcination was performed in air using covered aluminumoxide crucibles. Phase purity was checked by X-ray diffraction after each calcination step.

X-ray powder diffraction patterns were recorded at room temperature in the angular range $10° \leq 2\theta \leq 150°$ using a Seifert XRD TT 3003 diffractometer (Cu-$K_{\alpha 1,2}$ radiation). Angular steps of 0.01° and an integration time of 300 s per data point were chosen and a one dimensional single line semiconductor detector (Meteor 1D) was used. The Rietveld analysis was carried out with the FullProf suite [14,15]. The detailed refinement results for the $La_{2-x}Pr_xRu_{1-y}Ti_yO_5$ samples are listed in the Supplementary information [16]. Since the atomic form factors of La and Pr are almost identical, their occupancies were fixed to the nominal values. The Ru and Ti occupancies were refined assuming a complete site occupation. Deviations from the nominal values of less than 1% were detected, as listed in the supplemental material.

Magnetic suspectibilities $\chi = M/H$ were measured in the temperature range $2\ K \leq T \leq 400\ K$ with an applied field of $H = 1000$ Oe in field-cooled mode. The measurements were performed with a superconducting quantum interference device (SQUID) magnetometer (MPMS5-XL by Quantum Design). The powder samples were enclosed in gel capsules whose small contributions to the measured susceptibility was taken into account by an additional temperature independent χ_0-term during the data fitting procedure.

3. Results and discussion

3.1. Crystal structure

According to the X-ray diffraction data, single-phase polycrystalline samples were obtained for $0 \leq x \leq 0.75$ and $0 \leq y \leq 0.4$. Only traces of impurity phases $LaRuO_3$ or La_3RuO_7 (with contents well below 1%) were detected for the highest substitution levels. Both substitutions with Pr and Ti cause structural stress due to the slightly smaller ionic radii of the inserted ions compared to La and Ru [17]. However, the crystal structure changes differently for both kinds of substitution. Since the Pr ions are mainly located in the LaO layers and Ti can only be incorporated in the $LaRuO_4$ layers, a simultaneous substitution is expected to reach a limit at certain maximal levels x_{max} and y_{max} before structural stress impedes further substitution.

In Fig. 2 the measured pattern of $La_{1.5}Pr_{0.5}Ru_{0.8}Ti_{0.2}O_5$ ($x = 0.5$, $y = 0.2$) is depicted as a representative example along with the result of the Rietveld refinement. An excellent concordance of the refinement is obtained for all samples applying the ht crystal structure of La_2RuO_5 with monoclinic $P2_1/c$ symmetry as starting model. Details of the refinement results of two examples with high Pr and high Ti content are shown in Tables 1 and 2. The data for all samples are listed in the Supplementary material [16].

The evolution of the cell parameters for $La_{2-x}Pr_xRu_{1-y}Ti_yO_5$ is depicted in Fig. 3. The obtained values for the parameters *a*, *b*, *c*, and the values for the monoclinic angle β are shown in the panels (a)–(d), respectively. In addition to the co-doped samples the structural data of the single substituted La_2RuO_5 samples corresponding to $x = 0$ and $y = 0$ are included for comparison [3,4]. To illustrate the dependence on the two different substitution levels *x* and *y*, the three-dimensional plots are shown with a color coding depending on the cell-parameter value. Black arrows indicate increasing substitution levels.

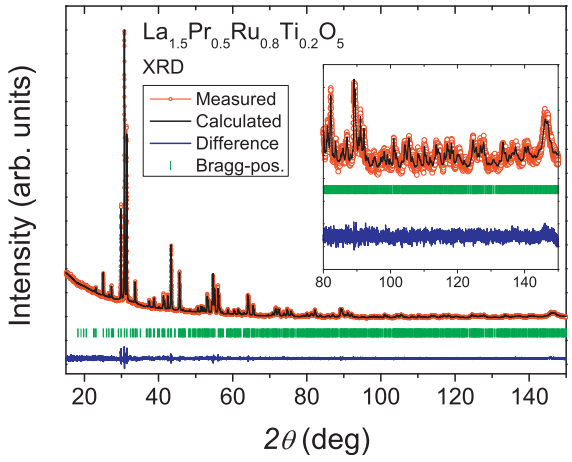

Fig. 2. Rietveld refinement of the X-ray diffraction pattern for $La_{1.5}Pr_{0.5}Ru_{0.8}Ti_{0.2}O_5$ ($x = 0.5$, $y = 0.2$), measured with Cu-$K_{\alpha 1,2}$ radiation at room temperature. In the inset a magnification of the range $80° \leq 2\theta \leq 150°$ is shown to illustrate the fit quality even for low intensities and strongly overlapping reflexes at higher diffraction angles.

Table 1
Cell parameters, fit residuals, atomic coordinates, and isotropic displacement factors (Å^2) derived from XRD-Rietveld refinement of $La_{1.25}Pr_{0.75}Ru_{0.80}Ti_{0.20}O_5$.

a (Å)	b (Å)	c (Å)	β (deg)
9.1212(2)	5.7994(1)	7.9400(2)	100.857(1)

R_p	R_{wp}	χ^2
1.52	2.02	2.75

Name	x	y	z	B_{iso}	Occ.
La/Pr	0.0456(2)	0.2385(7)	0.8779(2)	0.01(4)	1
La/Pr	0.6676(2)	0.2523(10)	0.5373(3)	0.85(5)	1
Ru	0.3502(3)	0.2515(15)	0.7131(5)	0.17(4)	0.80(1)
Ti	0.3502(3)	0.2515(15)	0.7131(5)	0.17(4)	0.20(1)
O1	0.9572(17)	0.1865(35)	0.1121(21)	0.65(17)	1
O2	0.3517(22)	0.1531(31)	0.9833(28)	0.65(17)	1
O3	0.2281(19)	0.5361(40)	0.7376(24)	0.65(17)	1
O4	0.2147(20)	0.0227(34)	0.6368(24)	0.65(17)	1
O5	0.4486(18)	−0.0300(41)	0.7130(29)	0.65(17)	1

For the a-axis (Fig. 3a), the doping effect of the smaller Pr ion compared to La is observed for all samples, causing a linear decrease of a with increasing x. In contrast, the a-axis length is barely affected by the value of y, i.e. by the titanium substitution level. The weak dependence on the Ti concentration can be seen in the projection of the data points onto the x–z-plane in the graph, where basically a linear decrease with increasing x can be observed. The smallest values for a are found for $x = 0.75$ and establish a limit of ≈9.12 Å, which is comparable to values obtained for pure rare-earth substitutions [3].

The b-axis (Fig. 3b) is decreasing linearly with both increasing Pr and Ti substitution levels. The effect of Ti substitution is more pronounced than for Pr substitution. The interplay between both substitutions generates an almost planar relation (Fig. 3b). The

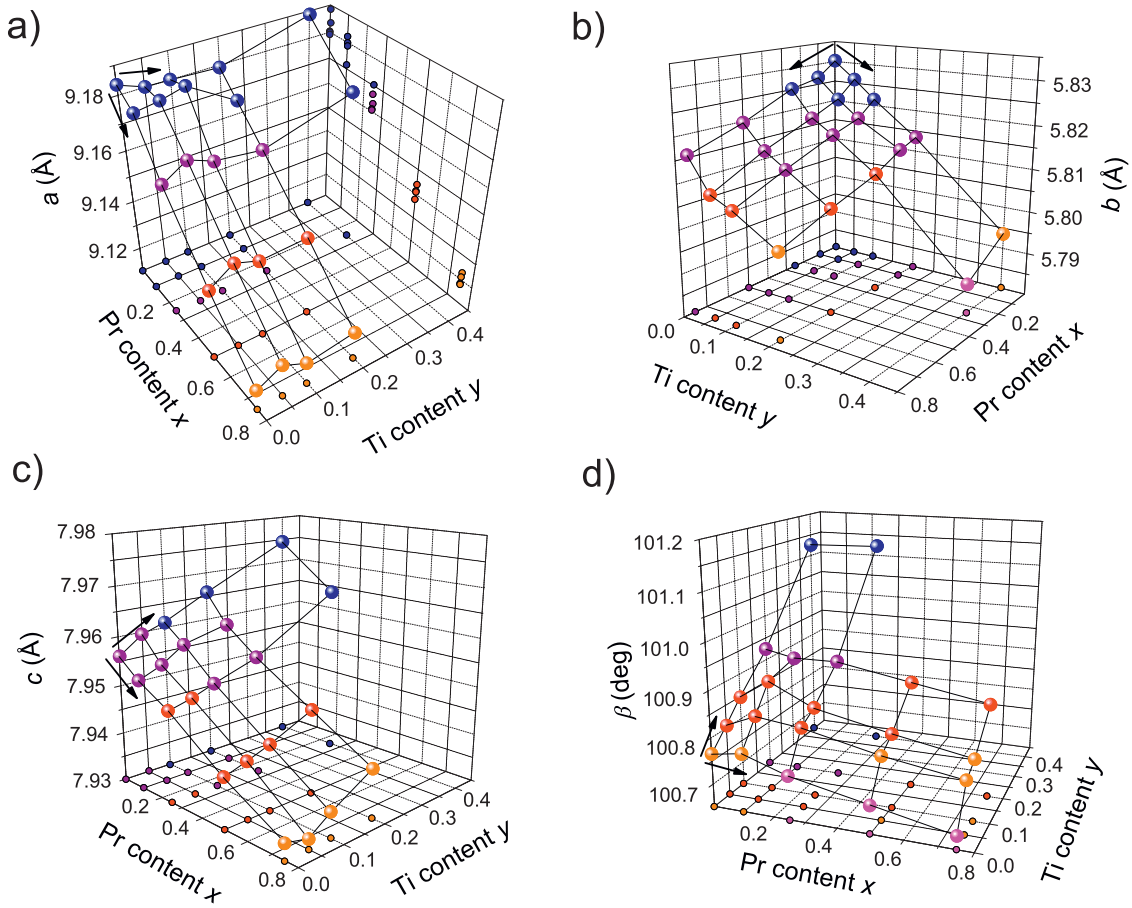

Fig. 3. Cell parameters for $La_{2-x}Pr_xRu_{1-y}Ti_yO_5$ derived from Rietveld analysis of powder XRD data measured at room temperature. The color-coded symbols represent the values of (a) length of the a-axis, (b) length of the b-axis, (c) length of the c-axis, and (d) monoclinic angle β. Error bars are smaller than the size of the symbols. (For interpretation of the references to color in figure legend, the reader is referred to the web version of the article.)

Table 2
Cell parameters, fit residuals, atomic coordinates, and isotropic displacement factors (Å^2) derived from XRD-Rietveld refinement of $La_{1.75}Pr_{0.25}Ru_{0.60}Ti_{0.40}O_5$.

a (Å)	b (Å)	c (Å)	β (deg)
9.1700(3)	5.7867(2)	7.9650(2)	101.131(1)

R_p	R_{wp}	χ^2
1.76	2.76	4.44

Name	x	y	z	B_{iso}	Occ.
La/Pr	0.0482(3)	0.2448(26)	0.8790(4)	0.33(7)	1
La/Pr	0.6695(3)	0.2506(23)	0.5396(5)	0.45(7)	1
Ru	0.3522(7)	0.2503(40)	0.7109(11)	0.33(8)	0.64(3)
Ti	0.3522(7)	0.2503(40)	0.7109(11)	0.33(8)	0.36(3)
O1	0.9305(29)	0.1406(50)	0.0866(37)	0.24(26)	1
O2	0.3740(31)	0.1852(44)	0.9595(38)	0.24(26)	1
O3	0.2246(27)	0.5072(63)	0.7351(37)	0.24(26)	1
O4	0.1819(34)	0.0507(56)	0.6225(42)	0.24(26)	1
O5	0.4751(37)	−0.0665(53)	0.7252(52)	0.24(26)	1

limit of structural stress is dominated by the Ti substitution, which impedes the synthesis of samples with both high Pr and Ti substitution levels. The smallest b-axis value is obtained for $La_{1.75}Pr_{0.25}Ru_{0.6}Ti_{0.4}O_5$ and corresponds to the limit ≈5.787 Å.

For the c-axis evolution (Fig. 3c) opposing effects for the different substitutions are observed. While with increasing Pr concentration the axis length is reduced, Ti substitution increases the c-axis. Since the two effects almost compensate each other, similar values for c are obtained when $x = y$. The c-axis values are limited between the Pr and Ti borders of ≈7.93 Å and ≈7.98 Å.

The monoclinic angle β (Fig. 3d) decreases for increasing Pr substitution, but, in contrast, increases for increasing Ti contents. The upper limit is given by the value obtained for the sample with highest Ti substitution level $La_2Ru_{0.55}Ti_{0.45}O_5$ and amounts to ≈101.18°.

The maximal and minimal values of the cell parameters define a stable regime, in which the La_2RuO_5 crystal structure can be synthesized. The limiting cell parameter for the maximum substitution is the b-axis length, because both Pr and Ti substitution induce a decrease. For the (average) Ru–O distances and the Ru–O–Ru bond angles only small changes in the range of 0.05 Å and 2° are observed [16]. The atomic coordinates of oxygen have rather large standard deviations when derived from X-ray diffraction data. Therefore, we only depict the Ru–Ru distances, which possess a higher accuracy. In Fig. 4 the Ru–Ru distances are shown (a) in the ab-plane and (b) along the c-axis. The distances in ab are in general slightly shorter than in c-direction, which is of importance for the magnetic phase transition. In accordance with the cell parameter b the Ru–Ru distance shown in Fig. 4a decreases with both increasing x and y. The Ru–Ru distance parallel to c also follows the behavior of the axis lengths, i.e. it increases with increasing Ti substitution level and decreases with increasing Pr concentration (Fig. 4b).

The Ru–O2–Ru (along c) and the Ru–O5–Ru (in the ab-plane) angles are of importance. Although the obtained values show severe scattering, it was found that both angles decrease with increasing Pr substitution level and increase with increasing Ti doping.

In summary, the effects of substitutions of La by Pr and Ru by Ti show an additive behavior resulting in planar relationships of the cell parameters. The Pr substitution mainly affects the LaO layers, where roughly two thirds of the Pr is incorporated, while the lower fraction of Pr is occupying the La-sites in the $LaRuO_4$ layers. This is leading to the observed strong reduction of the a-axis compared to the moderate decrease of the b- and c-axis. On the other hand, the Ti substitution does not significantly influence the a-axis due to the incorporation of Ti ions within the $LaRuO_4$ layers.

It should be mentioned that the relative changes of the cell parameters are within 1.5% compared to La_2RuO_5. This is a surprisingly small value and documents that the stability range of the La_2RuO_5 structure type is rather limited. But even these minor differences of the cell parameters are causing distinct changes of the physical properties of the substituted compounds, as shown for the magnetic properties in the following section.

3.2. Magnetic properties

The effect of the simultaneous substitution on the dimerization transition was investigated by measurements of the magnetic susceptibility. For pure La_2RuO_5 a magneto-structural transition caused by the Ru^{4+} ($S = 1$) spin pairing at $T_d = 161$ K is observed, which leads to the formation of non-magnetic singlets driven by the structural changes at T_d. This transition is preserved in the rare-earth substituted samples, but is progressively suppressed by increasing Ti substitution. For $y > 0.25$ the observed magnetic properties and the absence of a peak in the specific heat were ascribed to the appearance of only short-range ordered clusters of dimers in the low-temperature phase [3,4,6,12].

In Fig. 5a the magnetic susceptibilities for a constant Pr concentration ($x = 0.25$) are depicted. The χ curves are shifted by a

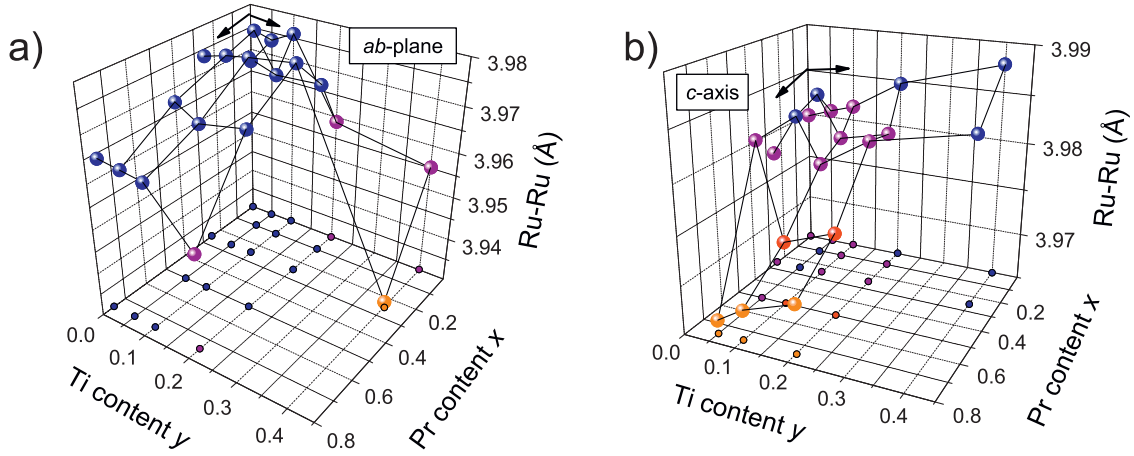

Fig. 4. Ru–Ru interatomic distances for $La_{2-x}Pr_xRu_{1-y}Ti_yO_5$ derived from Rietveld analysis of powder XRD data measured at room temperature. The color-coded symbols represent the values for Ru–Ru (a) in the ab-plane and (b) along the c-axis. (For interpretation of the references to color in figure legend, the reader is referred to the web version of the article.)

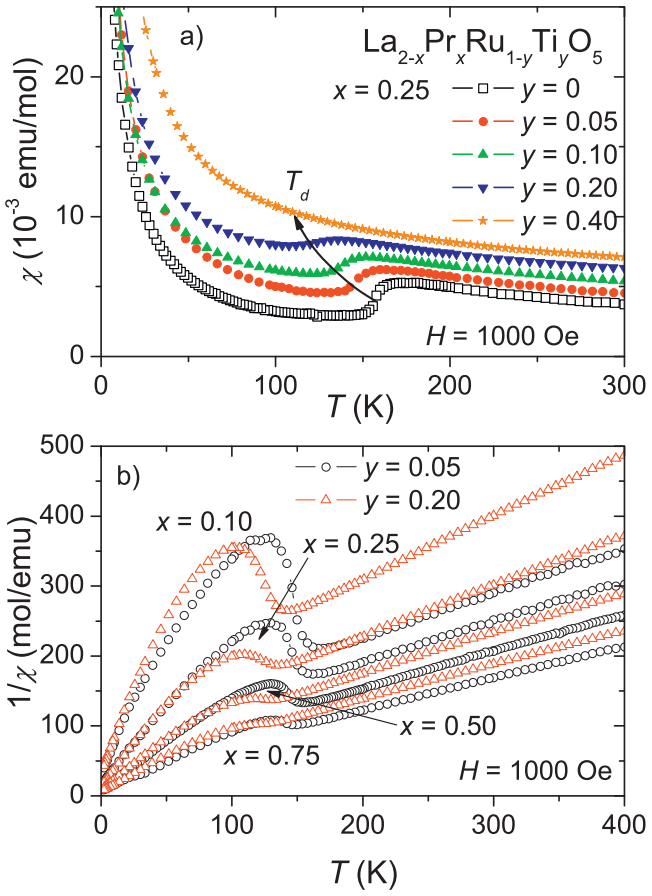

Fig. 5. (a) Temperature depending magnetic susceptibility $\chi = M/H$ of $La_{1.75}Pr_{0.25}Ru_{1-y}Ti_yO_5$ applying an external field of $H = 1000$ Oe. The curves are shifted by a constant value for better comparability. The arrow marks the shift of the transition temperature T_d upon Ti substitution. (b) Thermal behavior of the inverse magnetic susceptibility $1/\chi$ of $La_{2-x}Pr_xRu_{0.95}Ti_{0.05}O_5$ and $La_{2-x}Pr_xRu_{0.8}Ti_{0.2}O_5$ at $H = 1000$ Oe.

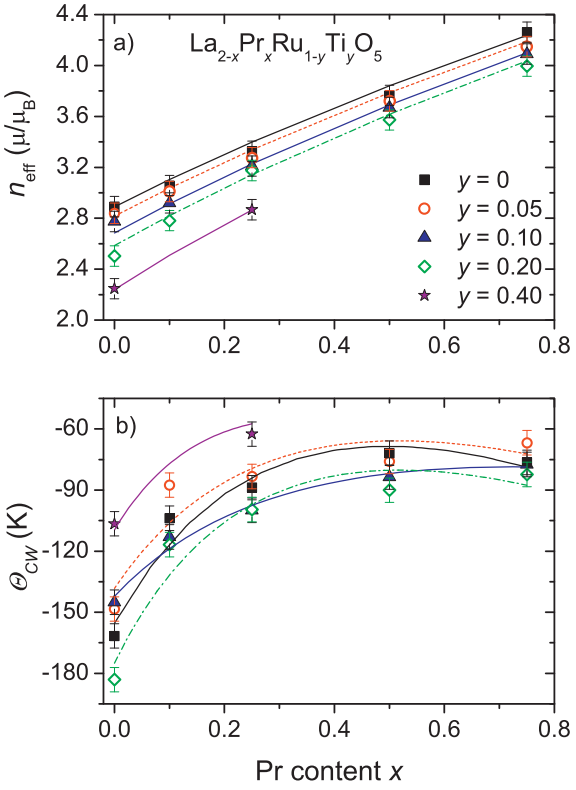

Fig. 6. (a) Effective magnetic moments in Bohr magnetons derived from Curie–Weiss fits of $1/\chi$ in the temperature range 200–400 K. The dashed lines represent the sum of the moments according to Eq. (1) using the spin-only value for Ru^{4+} and the free-ion approximation value for Pr^{3+}. (b) Curie–Weiss temperatures obtained from the fit of $1/\chi$ in the temperature range 200–400 K. The lines represent Θ_{CW} values calculated with Eq. (2).

constant value for better comparability. The strong increase at very low temperatures can be ascribed to both the paramagnetic Pr^{3+} ions and emerging unpaired Ru^{4+} spin moments in the range of a few percent. In the paramagnetic regime above T_d susceptibilities for $La_{1.75}Pr_{0.25}Ru_{1-y}Ti_yO_5$ indicate a slight reduction of the paramagnetic moment and changes of the Curie–Weiss temperature with increasing Ti substitution level. A diminishing of the transition step is observed in agreement with the findings for $La_2Ru_{1-y}Ti_yO_5$ [4]. The transition step becomes broader with increasing y and its height declines progressively until it vanishes for $y = 0.40$. This value is slightly lower than the one obtained for the $La_2Ru_{1-y}Ti_yO_5$, i.e. samples without Pr substitution [4]. Due to the Pr incorporation the borders of the phase diagram (y, T) introduced in Ref. [4] is shifted to lower y-values.

The suppression of the susceptibility step as a consequence of the Ti incorporation is also visible for the inverse susceptibility, which is depicted in Fig. 5b. The $1/\chi$ curves for two Ti substitutions, $y = 0.05$ and $y = 0.20$, are shown for different Pr substitution levels x. In the paramagnetic range above 200 K a linear behavior in agreement with a Curie–Weiss law is observed. The increasing Pr contribution to the total magnetic moment is reflected by the decreasing slope of the linear regions. Furthermore, the higher Ti substitution level generates a stronger splitting of the curves for the ht-phase. In turn, the decreasing upturn caused by the dimerization transition is correlating with the behavior observed for the solely Ti substituted samples reflecting the suppression of the long-range singlet formation [4].

The high temperature regions above 200 K of the inverse susceptibilies can be described using a Curie–Weiss fit $\chi = C/(T - \Theta_{CW}) + \chi_0$. The temperature independent χ_0 was used to account for diamagnetic and possible van-Vleck contributions as well as the gel capsules used to enclose the samples. The values of χ_0 were found to decrease from roughly 10^{-4} to 10^{-5} emu/mol with increasing substitution levels x and y, which indicates either rising diamagnetic and/or decreasing van-Vleck contributions. The effective magnetic moments n_{eff}, which were derived from the obtained Curie constant values C, are shown in Fig. 6a in units of Bohr magneton μ_B. The solid and dashed lines represent the calculated $n_{eff,total}$ according to

$$n_{eff,total} = \sqrt{(1-y)\cdot n_{eff}^2(Ru^{4+}) + x\cdot n_{eff}^2(Pr^{3+})}, \quad (1)$$

where x and y are the corresponding Pr and Ti substitution levels. This equation implies completely independent contributions of the two types of paramagnetic ions. The Ru moment $n_{eff}(Ru^{4+})$ is taken from the fit of the pure La_2RuO_5 amounting to 2.89 μ_B. This value is in good agreement with the spin only value 2.83 μ_B expected for $S = 1$. The magnetic moment of Pr was calculated applying the free-ion approximation ($n_{eff}(Pr^{3+}) = 3.578\mu_B$) [18]. The good agreement of the magnetic moments obtained from the Curie–Weiss fit with the values calculated using Eq. 1 is evident from Fig. 6a. The deviations are within the range of the error bars proving that the assumed additive behavior of the contribution of Ru^{4+} and Pr^{3+} to the total magnetic moment is correct.

The Curie–Weiss temperatures Θ_{CW}, which are depicted in Fig. 6b, were used to investigate in more detail the character of the paramagnetic ht-phase. The negative sign of Θ_{CW} indicates the

presence of antiferromagnetic interactions, as e.g. $\Theta_{CW} \approx -162$ K for the La_2RuO_5 sample. The absolute value is mirroring the interaction strength, which was found to decrease with increasing substitution level x, i.e. with a higher content of paramagnetic rare-earth ions. On the other hand, the Ti substitution leads to a change of the interaction strength due to structural deformations and the dilution of the interacting Ru-spin moments by the diamagnetic Ti^{4+}. In detail, the Ru–O bond lengths get reduced with increasing Ti incorporation and in turn the exchange interactions between the Ru-centers become stronger. This effect is increasing the absolute value of Θ_{CW} in the range $0.1 < y < 0.25$ reaching a minimum of approximately -185 K at $y = 0.25$. Upon higher Ti substitution levels a decrease of the absolute value is found [4]. Starting at $y = 0.25$ the increasing dilution of the Ru-centers starts to dominate the magnetic exchange and, hence, explains the strong decrease of $|\Theta_{CW}|$. For the co-substituted samples the Θ_{CW} values are shown in Fig. 6b. They reveal a decreasing absolute value for increasing x and constant y. Furthermore, for constant x the Curie–Weiss temperatures behave according to the solely Ti substitution, i.e. for $y = 0.2$ always a minimum is observed in the graph. This behavior of Θ_{CW} indicates the change from a long-range dimerized lt-phase with singlet ground state to a phase with only short-range ordering of dimers in clusters.

The lines in Fig. 6b represent a fit of Θ_{CW} for two antiferromagnetically interacting sublattices A (Ru^{4+}) and B (Pr^{3+}) according to the equation [19]:

$$\Theta_{CW} = \frac{2\lambda_{AB}C_AC_B - \lambda_{AA}C_A^2 - \lambda_{BB}C_B^2}{C_A + C_B}. \quad (2)$$

The Curie constants C_A and C_B were calculated from the effective magnetic moments (Eq. (1)). The parameters λ_{AA} and λ_{BB} correspond to interactions within the separate sublattices of Ru^{4+} and Pr^{3+}, respectively, while λ_{AB} describes the interaction between these two lattices. The interaction strength W_{AB} was calculated by $W_{AB} = -\lambda_{AB}$ according to Ref. [19]. The other interaction strengths were calculated by the combination of W_{AB} multiplied with the corresponding parameter λ ($W_{AA} = \lambda_{AA} \cdot W_{AB}$ and $W_{BB} = \lambda_{BB} \cdot W_{AB}$). The values of the λ parameters were obtained from least-squares fits of the Curie–Weiss temperatures for constant Ti substitution level. The results are the solid and dashed curves shown in Fig. 6b. Since only a limited number of data points are available for the fit, the absolute values are just taken as a measure of the involved interactions. For $y = 0.40$ only two data points are available. Therefore, the parameters λ_{AB} and λ_{BB} were taken from the $y = 0.05$ fit and only λ_{AA} was refined.

Good agreement between the measured Θ_{CW} values and the fit was obtained. The sign of all interaction strengths W is negative, which reflects antiferromagnetic interactions both within the sublattices and between them, in agreement with the results given in Ref. [3] and also in accordance with the negative Curie–Weiss temperatures. The absolute values of the interaction strength behave according to $W_{AA} > W_{BB} >> W_{AB}$ (or $W(\mathrm{Ru-Ru}) > W(\mathrm{Pr-Pr}) >> W(\mathrm{Ru-Pr})$). Thus, the interactions within the sublattices are much stronger by roughly two orders of magnitude than between them. It is therefore justified to describe the overall magnetic behavior by two almost independent sublattices. The values of W show a local maximum for the Ti substitution level $y = 0.2$ and a strong decrease for $y = 0.40$. This reflects the behavior for the pure Ti substitution, where a maximum of Θ_{CW} is found close to $y \approx 0.25$ [4]. In general, the (antiferro-)magnetic interactions are diminishing in accordance with the decreasing absolute values of Θ_{CW}. Simultaneously doping of Pr ions into $LaRuO_4$ does therefore not change the impact of Ti substitution on the system.

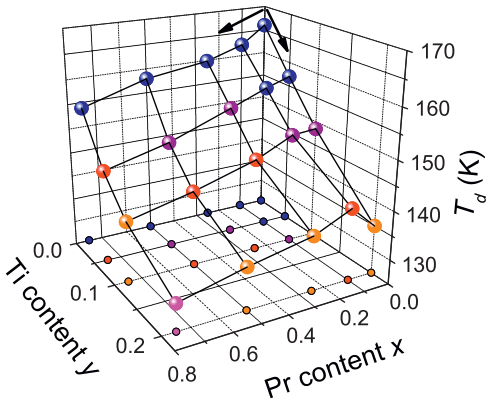

Fig. 7. Dimerization temperatures T_d obtained from the magnetic susceptibility data of $La_{2-x}Pr_xRu_{1-y}Ti_yO_5$.

From the inverse susceptibilities, the dimerization temperatures were obtained, using the onsets of the transition anomalies (see Fig. 7). Since no transition was observed for the sample $La_{1.75}Pr_{0.25}Ru_{0.60}Ti_{0.40}O_5$, T_d is only shown for $y \leq 0.20$. Within this range the transition temperature decreases linearly in both directions with increasing substitution levels. The effect of the Ti substitution is more pronounced than of the Pr substitution (steeper slope in y direction in Fig. 7). This can be explained by different origins for the T_d reduction. Pr substitution leads to a decrease by increasing delocalization of the Ru electrons. This delocalization is caused by an electronic band broadening resulting from slight changes of the crystal structure [3,6]. On the other hand, the Ti substitution directly impedes the Ru dimerization by the dilution of the magnetic Ru centers and, therefore, provides a more pronounced influence on the phase transition [4]. Since the structural parameters change according to Vegard's law, a linear decrease of T_d is very reasonable. The simultaneous replacement of La and Ru leads to the obtained change of T_d depending on the particular substitution levels x and y, because both substitutions alter the structural and the magnetic properties almost independently.

4. Summary and conclusions

The simultaneous substitution of La by Pr and Ru by Ti in La_2RuO_5 was successfully carried by a soft-chemistry synthesis route. Samples according to the sum formula $La_{2-x}Pr_xRu_{1-y}Ti_yO_5$ were synthesized for a large composition range $0 \leq x \leq 0.75$ and $0 \leq y \leq 0.4$. The upper substitution limits reflect the increasing structural stress caused by the differing ionic radii of the substitution.

The polycrystalline samples were investigated by X-ray powder diffraction at room temperature in combination with Rietveld refinements. The cell parameters reflect a completely additive behavior with respect to the changes obtained for the pure Pr and Ti substitutions. This finding can be explained taking into account the layered structure of La_2RuO_5. While Pr ions are predominantly occupying the LaO layers, Ti ions are located on the Ru sites within the $LaRuO_4$ layers. The simultaneous substitution leads to a certain degree of compensation of the cell-parameter changes, which results in a large regime of x and y. Only the b-axis is shortened by both substitutions, which limits the range of simultaneously high substitution levels for Pr and Ti ($x \leq 0.5$ and $y \leq 0.3$).

The magnetic susceptibilities can be explained assuming a coexistence of two only weakly interacting magnetic sublattices formed by the Pr^{3+}- and Ru^{4+}-ions, respectively. The Curie–Weiss temperatures Θ_{CW} exhibit largest negative values for medium titanium contents. Increasing (absolute) values found for $0 \leq y \leq 0.2$ are caused by increasing antiferromagnetic interactions due to the decrease of interatomic distances. The decrease of $|\Theta_{CW}|$ for $y > 0.2$ can be explained by the dominating dilution of

the magnetic Ru-centers by non-magnetic Ti and the formation of short-range ordered clusters of dimers [4].

A magnetic phase transition reflecting a Ru–Ru spin pairing in the lt-phase is observed for all samples with $y < 0.4$. While the rare-earth substitution has no direct effect on the Ru–Ru dimerization, Ti ions impede this process for substitution levels of $y \geq 0.4$. The Pr substitution disfavours the formation of spin dimers by the broadening of the electronic Ru bands due to structural changes, which increase the delocalization of the Ru spin moments. In contrast, Ti ions directly interrupt the dimerization and therefore reduce the number of spin singlets. As the Pr and the Ti substitutions do not mutally affect each other, linear changes with both x and y are found for all parameters investigated.

Acknowledgements

The authors gratefully acknowledge Dana Vieweg for the SQUID measurements. This work was financially supported by the graduate school (Resource strategy concepts for sustainable energy systems) of the Institute of Materials Resource Management (MRM) of the University of Augsburg.

References

[1] P. Khalifah, R. Osborn, Q. Huang, H.W. Zandbergen, R. Jin, Y. Liu, D. Mandrus, R.J. Cava, Science 297 (2002) 2237–2240.
[2] S.G. Ebbinghaus, S. Riegg, T. Götzfried, A. Reller, Eur. Phys. J. ST 180 (2010) 91–116.
[3] S. Riegg, U. Sazama, M. Fröba, A. Reller, S.G. Ebbinghaus, Phys. Rev. B 84 (2011) 014403.
[4] S. Riegg, S. Widmann, A. Günther, H.-A. Krug von Nidda, A. Reller, A. Loidl, S.G. Ebbinghaus, J. Phys.: Condens. Matter 25 (2013) 126002.
[5] S. Riegg, A. Reller, S.G. Ebbinghaus, J. Solid State Chem. 188 (2012) 17–25.
[6] S. Riegg, A. Günther, H.-A. Krug von Nidda, M.V. Eremin, A. Reller, A. Loidl, S.G. Ebbinghaus, Eur. Phys. J. B 85 (2012) 413.
[7] S.K. Malik, D.C. Kundaliya, R.D. Kale, Solid State Commun. 135 (2005) ‘ 166–169.
[8] S.G. Ebbinghaus, Acta Crystallogr. Sect. C 61 (2005) i96–i98.
[9] V. Eyert, S.G. Ebbinghaus, T. Kopp, Phys. Rev. Lett. 96 (2006) 256401.
[10] V. Eyert, S.G. Ebbinghaus, Prog, Solid State Chem. 35 (2007) 433–439.
[11] Wu Hua, Z. Hu, T. Burnus, J.D. Denlinger, P.G. Khalifah, D.G. Mandrus, L.-Y. Jang, H.H. Hsieh, A. Tanaka, K.S. Liang, J.W. Allen, R.J. Cava, D.I. Khomskii, L.H. Tjeng, Phys. Rev. Lett. 96 (2006) 256402.
[12] S. Riegg, A. Günther, H.-A. Krug von Nidda, A. Loidl, M.V. Eremin, A. Reller, S.G. Ebbinghaus, Phys. Rev. B 86 (2012) 115125.
[13] P. Boullay, D. Mercurio, A. Bencan, A. Meden, G. Drazic, M. Kosec, J. Solid State Chem. 170 (2003) 294–302.
[14] H.M. Rietveld, J. Appl. Crystallogr. 2 (1969) 65–71.
[15] J. Rodriguez-Carvajal, Physica B 192 (1993) 55–69.
[16] The crystal structure data obtained from the Rietveld analysis for the $La_2 - xPr_x$-$Ru_1 - yTi_yO_5$ samples are listed in the supplementary information: http://dx.doi.org/10.1016/j.materresbull.2013.07.054.
[17] R.D. Shannon, Acta Crystallogr. Sect. A 32 (1976) 751–767.
[18] H. Lueken, Magnetochemie, Teubner, Stuttgart, Leipzig, 1999.
[19] J.B. Goodenough, Magnetism the Chemical Bond, in: Interscience, Wiley, New York/London, 1963.